



**HAL**  
open science

## Camelid nanobodies used as crystallization chaperones for different constructs of PorM, a component of the type IX secretion system from *Porphyromonas gingivalis*

Yoan Duhoo, Jennifer Roche, Thi Trang Nhung Trinh, Aline Desmyter, Anaïs Gaubert, Christine Kellenberger, Christian Cambillau, Alain Roussel, Philippe Leone

### ► To cite this version:

Yoan Duhoo, Jennifer Roche, Thi Trang Nhung Trinh, Aline Desmyter, Anaïs Gaubert, et al.. Camelid nanobodies used as crystallization chaperones for different constructs of PorM, a component of the type IX secretion system from *Porphyromonas gingivalis*. *Acta crystallographica Section F : Structural biology communications* [2014-..], 2017, 73 (5), pp.286 - 293. 10.1107/S2053230X17005969 . hal-01802819

**HAL Id: hal-01802819**

**<https://hal.science/hal-01802819>**

Submitted on 8 Jun 2018

**HAL** is a multi-disciplinary open access archive for the deposit and dissemination of scientific research documents, whether they are published or not. The documents may come from teaching and research institutions in France or abroad, or from public or private research centers.

L'archive ouverte pluridisciplinaire **HAL**, est destinée au dépôt et à la diffusion de documents scientifiques de niveau recherche, publiés ou non, émanant des établissements d'enseignement et de recherche français ou étrangers, des laboratoires publics ou privés.



# Camelid nanobodies used as crystallization chaperones for different constructs of PorM, a component of the type IX secretion system from *Porphyromonas gingivalis*

Yoan Duhoo,<sup>a,b</sup> ‡ Jennifer Roche,<sup>a,b</sup> ‡ Thi Trang Nhung Trinh,<sup>a,b</sup> ‡ Aline Desmyter,<sup>a,b</sup>  
Anaïs Gaubert,<sup>a,b</sup> Christine Kellenberger,<sup>a,b</sup> Christian Cambillau,<sup>a,b</sup> Alain  
Roussel<sup>a,b,\*</sup> and Philippe Leone<sup>a,b,\*</sup>

Received 25 January 2017

Accepted 19 April 2017

Edited by R. L. Stanfield, The Scripps Research Institute, USA

‡ These authors contributed equally to this work.

**Keywords:** camelid nanobodies; type IX secretion system; crystallization chaperones; PorM; *Porphyromonas gingivalis*.

**PDB references:** nb01, 5lz0; nb02, 5lmw; nb19, 5lmj; nb130, 5fwo

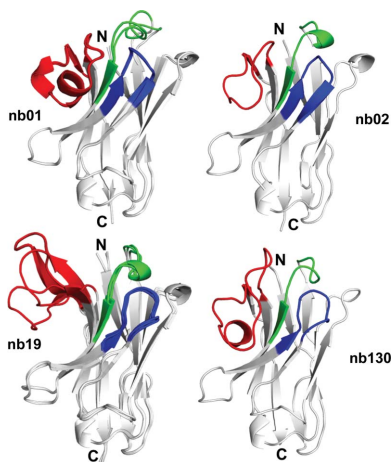
**Supporting information:** this article has supporting information at journals.iucr.org/f

<sup>a</sup>Centre National de la Recherche Scientifique, Architecture et Fonction des Macromolécules Biologiques, UMR 7257, Marseille, France, and <sup>b</sup>Aix-Marseille Université, Architecture et Fonction des Macromolécules Biologiques, UMR 7257, Marseille, France. \*Correspondence e-mail: alain.roussel@afmb.univ-mrs.fr, philippe.leone@afmb.univ-mrs.fr

PorM is a membrane protein that is involved in the assembly of the type IX secretion system (T9SS) in *Porphyromonas gingivalis*, a major bacterial pathogen that is responsible for periodontal disease in humans. In the context of structural studies of PorM to better understand T9SS assembly, four camelid nanobodies were selected, produced and purified, and their specific interaction with the N-terminal or C-terminal part of the periplasmic domain of PorM was investigated. Diffracting crystals were also obtained, and the structures of the four nanobodies were solved by molecular replacement. Furthermore, two nanobodies were used as crystallization chaperones and turned out to be valuable tools in the structure-determination process of the periplasmic domain of PorM.

## 1. Introduction

Periodontal disease is one of the most frequently occurring infectious diseases in humans (Armitage, 1996). The main microorganism responsible for periodontitis and gingivitis is the oral pathogenic bacterium *Porphyromonas gingivalis*. Infection by this Gram-negative bacterium causes severe lesions in periodontal tissues, leading to destruction of the alveolar bone and the tooth-supporting structure in the most severe cases. This damage is induced by a cocktail of specialized toxin proteins secreted by *Porphyromonas*, called gingipains. Gingipains act as adhesins and/or proteases that help the bacterium to adhere to periodontal tissues and to promote the invasion of gingival tissues by the degradation of matrix proteins, fibrinogen and collagen. The active release of gingipains at the bacterial cell surface is catalyzed by a recently identified protein complex called the type IX secretion system (T9SS; Sato *et al.*, 2010). The T9SS is composed of 10–14 subunits, encoded by the *por* genes, that are thought to assemble a transenvelope channel that specifically recruits the gingipains and transports them to the cell surface, where they are processed to become active (by cleavage of a C-terminal sequence and glycosylation). Interestingly, four of these proteins, PorK, PorL, PorM and PorN, are sufficient to assemble a stable complex of ~1.2 MDa that resists native PAGE analyses (Sato *et al.*, 2010). In a recent study (Vincent *et al.*, 2017), we have shown that PorK is a lipoprotein anchored



in the outer membrane that interacts strongly with the periplasmic protein PorN, and that PorL and PorM are inner membrane proteins which interact with each other *via* their transmembrane segments. In addition to its transmembrane segment, PorM possesses a long periplasmic domain of nearly 500 residues which is thought to link the inner and outer membrane subcomplexes.

A crystallization strategy for PorM is to use camelid nanobodies as crystallization chaperones. In addition to conventional antibodies, members of the Camelidae family possess a set of unusual antibodies that consist only of heavy chains; the constant domain is missing, and they are therefore named heavy-chain-only antibodies or nanobodies (Hamers-Casterman *et al.*, 1993). These antibodies offer a very interesting new tool in scientific research, as they contain variable domains (VHHs) that are fully responsible for and are fully capable of recognizing and binding to antigens. The variable domains are also more hydrophilic than their IgG counterparts, as they are not required to bind to a complementary domain of a light chain (Spinelli *et al.*, 1996). Moreover, they are very stable, and owing to their rather small size (14 kDa) they are able to bind to epitopes within clefts (Desmyter *et al.*, 1996) that are more difficult to reach for larger antibodies. Both their single-domain nature and their lack of glycosylation allow them to be produced at high levels using bacterial expression systems.

Using the nanobody platform of our laboratory, we were able to raise four nanobodies against the periplasmic domain of PorM (residues 36–516). Here, we present an investigation of their binding specificities and their crystal structures. Moreover, diffracting crystals of the N- and C-terminal parts of PorM in complex with their respective nanobodies were obtained. These crystals were essential in the structure-determination process of the targets, validating the strategy of using nanobodies as crystallization chaperones.

## 2. Materials and methods

### 2.1. Generation of nanobodies against pPorM

Four injections of 0.5 mg purified periplasmic domain of PorM (pPorM) in 10 mM HEPES pH 7.4, 150 mM NaCl were performed subcutaneously at one-week intervals followed by a fifth injection two weeks later in one llama (*Llama glama* from Ardèche Lamas, France). Lymphocytes were isolated from blood samples obtained 5 d after the last immunization. The cDNA was synthesized from purified total RNA by reverse transcription and was used as a template for PCR amplification to amplify the sequences corresponding to the variable domains of the heavy-chain antibodies. PCR fragments were then cloned into the phagemid vector pHEN4 (Arbabi Ghahroudi *et al.*, 1997) to create a nanobody phage-display library. The selection and screening of nanobodies were performed as described previously (Desmyter *et al.*, 2013). Three rounds of panning resulted in the isolation of pPorM-specific binders. After sequence analysis, four different positive clones, nb01, nb02, nb06 and nb19, were chosen to be

subcloned into pHEN6 expression vector downstream of the pelB signal peptide and fused to a C-terminal 6×His tag (Conrath *et al.*, 2009).

A nanobody phage-display naïve library was generated by the same procedure as described above, starting from the blood of several non-immunized animals: three camels (*Camelus dromedarius* from C. Gutierrez at Universidad de Las Palmas de Gran Canaria, Spain) and four llamas (*L. glama* from Capralogics Inc., USA). Three rounds of panning resulted in the isolation of pPorM-specific binders. After sequence analysis, three different positive clones, nb103, nb130 and nb105, were found corresponding to nb02, nb06 and nb19, respectively, from the immunized library. Clone nb130 was subcloned into pHEN6 expression vector.

### 2.2. Production and purification of nanobodies

The expression and purification of the nanobodies was performed as described previously (Conrath *et al.*, 2009). The periplasmic fraction was extracted by osmotic shock and the recombinant nanobodies were purified on a 5 ml Ni-NTA column (GE Healthcare) in 50 mM sodium/potassium phosphate pH 8.0, 300 mM NaCl, 10% glycerol. The fractions eluted in 250 mM imidazole were concentrated by centrifugation using an Amicon Ultra 10 kDa cutoff concentrator prior to being loaded onto a HiLoad 10/30 Superdex 75 pg gel-filtration column (GE Healthcare) equilibrated in phosphate-buffered saline (PBS). The purified nanobodies were concentrated by centrifugation; their concentration was determined by measuring the absorbance at 280 nm with a NanoDrop 2000 (Thermo Scientific).

### 2.3. Cloning, production and purification of PorM constructs

pPorM and its trypsinized fragment (pPorM-T) were produced as described previously (Stathopoulos *et al.*, 2015). The sequence of pPorM-T was deduced by N-terminal Edmann sequencing and peptide mass fingerprinting (results not shown), and corresponds to the C-terminal part of pPorM (residues 225–516). This sequence (hereafter denoted pPorM-Cter) and the sequence corresponding to the remaining N-terminal part of pPorM (residues 44–217; hereafter denoted pPorM-Nter) were cloned into the pET-28a+ derivative vector pLIC03. The pPorM-Cter and pPorM-Nter proteins were produced and purified using the same protocol as for pPorM.

### 2.4. Purification of nanobodies in complex with PorM constructs

The nanobodies and the PorM constructs pPorM-Nter and pPorM-Cter were first purified independently by nickel-affinity chromatography as described previously. The proteins were then mixed in a molar ratio of 1:1.2 (PorM constructs: nanobodies) and left for 15 min at room temperature to form the following complexes: pPorM-Nter in complex with nb01 or nb02, and pPorM-Cter in complex with nb19 or nb130. The complexes were purified on a HiLoad 16/60 Superdex 75 pg gel-filtration column (GE Healthcare) equilibrated in 10 mM HEPES pH 7.5, 150 mM NaCl. The purified complexes were

**Table 1**  
Data-collection and refinement statistics.

Values in parentheses are for the highest resolution shell.

	nb01	nb02	nb19	nb130
Crystallization condition	0.1 M trisodium citrate pH 5.5, 20%(w/v) PEG 3000	0.1 M trisodium citrate pH 5.5, 20% PEG 3000	0.1 M HEPES pH 4.5–5.5, 0.4–1.2 M NaH <sub>2</sub> PO <sub>4</sub> , 0.4–1.2 M KH <sub>2</sub> PO <sub>4</sub>	0.2 M diammonium citrate pH 5.0, 20%(w/v) PEG 3350
Protein concentration (mg ml <sup>-1</sup> )	14.0	13.0	10.1	16.0
Data collection				
Cryoprotectant	20%(v/v) polypropylene glycol	10% glycerol	30%(v/v) glycerol	20%(v/v) glycerol
Diffraction source	ID-23, ESRF	ID-23, ESRF	ID-29, ESRF	PROXIMA-2, SOLEIL
Space group	C2	P4 <sub>3</sub> 2 <sub>1</sub> 2	P4 <sub>1</sub> 2 <sub>1</sub> 2	P6 <sub>1</sub> 22
<i>a</i> , <i>b</i> , <i>c</i> (Å)	78.33, 65.83, 48.31	65.68, 65.68, 88.80	113.26, 113.26, 153.45	54.54, 54.54, 126.72
$\alpha$ , $\beta$ , $\gamma$ (°)	90, 95.89, 90	90, 90, 90	90, 90, 90	90, 90, 120
Resolution (Å)	28.8–1.60 (1.69–1.60)	46.44–1.50 (1.58–1.50)	48.1–2.10 (2.21–2.10)	47.23–1.70 (1.79–1.70)
Wavelength (Å)	0.87260	0.8729	1.07224	0.9801
Unique reflections	31426 (4389)	31805 (4532)	58799 (8431)	13038 (1821)
Multiplicity	5.3 (5.5)	6.8 (6.5)	8.7 (8.2)	21.0 (21.1)
Completeness (%)	97.7 (94.1)	99.9 (99.4)	99.9 (99.9)	99.9 (99.6)
$\langle I/\sigma(I) \rangle$	10.5 (1.7)	22.0 (1.7)	15.0 (1.7)	24.6 (2.4)
$R_{\text{meas}}^{\dagger}$ (%)	11.8 (111.1)	5.1 (124.5)	7.9 (144.0)	8.5 (139.6)
$R_{\text{p.i.m.}}^{\ddagger}$ (%)	5.1 (46.6)	1.9 (48.2)	2.6 (47.9)	1.9 (30.2)
CC <sub>1/2</sub> <sup>§</sup>	0.997 (0.693)	1.000 (0.627)	0.998 (0.652)	0.999 (0.850)
Mosaicity (°)	0.21	0.23	0.05	0.15
Solvent content (%)	40.6	63.3	70.8	37.2
Molecular replacement				
PDB code of starting model	4tvs	4qgy	4hem	4fhb
Refinement and model quality				
Resolution (Å)	27.2–1.6	19.58–1.5	46.6–2.1	44.2–1.7
No. of reflections	31426	31733	58723	12963
$R_{\text{cryst}}/R_{\text{free}}^{\parallel}$ (%)	20.5/23.2 1	18.8/19.6	18.8/21.0	18.6/22.2
No. of atoms				
Protein [chain(s) in asymmetric unit]	1902 [2]	957 [1]	3833 [4]	1000 [1]
Water/ion/ligand	251/–/–	213/–/6	404/55/–	108/–/–
Average <i>B</i> factors (Å <sup>2</sup> )				
Protein	21.4	27.5	68.5	33.4
Water/ion/ligand	32.9/–/–	46.4/–/29.9	73.0/81.4/–	46.1/–/–
R.m.s.d. <sup>††</sup>				
Bonds (Å)	0.01	0.01	0.01	0.01
Angles (°)	0.97	0.98	1.11	1.05
Ramachandran plot (%)				
Most favoured regions	96.3	94.0	97.9	97.5
Additionally allowed regions	3.7	5.2	1.7	2.5
PDB code	5lz0	5lmw	5lmj	5fwo

	nb01–pPorM-Nter	nb130–pPorM-Cter		
Crystallization condition	0.1 M bis-tris pH 7.0, 25%(w/v) PEG 3350	0.1 M HEPES pH 7.5, 0.2 M NaCl, 25%(w/v) PEG 3350	0.2 M ammonium citrate tribasic pH 7.0, 20%(w/v) PEG 3350	
Protein concentration (mg ml <sup>-1</sup> )	10.0	10.1	10.1	10.1
Data collection				
Cryoprotectant	10%(v/v) glycerol	20%(v/v) glycerol	10%(v/v) PEG 400	10%(v/v) PEG 400, 30%(w/v) PEG 3350
Diffraction source	PROXIMA-1, SOLEIL	PROXIMA-1, SOLEIL	PROXIMA-1, SOLEIL	PROXIMA-1, SOLEIL
Space group	P2 <sub>1</sub>	P2	P2 <sub>1</sub>	P1
<i>a</i> , <i>b</i> , <i>c</i> (Å)	80.35, 100.12, 80.41	64.05, 78.11, 76.09	64.87, 157.40, 77.37	55.24, 77.18, 156.30
$\alpha$ , $\beta$ , $\gamma$ (°)	90, 93.82, 90	90, 104.69, 90	90, 105.51, 90	90.24, 91.75, 97.16
Resolution (Å)	42.47–2.40 (2.53–2.40)	40–2.50 (2.63–2.50)	40–2.15 (2.27–2.15)	40–2.10 (2.21–2.10)
Wavelength (Å)	0.97857	0.97857	0.97857	0.97857
Unique reflections	49059 (7020)	25205 (3620)	80438 (11626)	145898 (21179)
Multiplicity	6.9 (6.8)	3.8 (3.7)	4.2 (4.3)	2.9 (2.9)
Completeness (%)	98.3 (96.7)	99.4 (97.7)	99.3 (98.7)	97.6 (96.8)
$\langle I/\sigma(I) \rangle$	11.6 (1.0)	8.6 (2.0)	12.5 (1.8)	27.5 (2.0)
$R_{\text{meas}}^{\dagger}$ (%)	7.8 (203.3)	12.1 (70.6)	8.1 (92.1)	6.5 (76.4)
$R_{\text{p.i.m.}}^{\ddagger}$ (%)	3.0 (77.4)	6.2 (36.2)	3.9 (44.0)	3.7 (43.3)
CC <sub>1/2</sub> <sup>§</sup>	0.999 (0.755)	0.995 (0.766)	0.999 (0.660)	0.998 (0.647)
Mosaicity (°)	0.05	0.15	0.15	0.19
Solvent content (%)	43.4	48.9	50.6	43.1

<sup>†</sup>  $R_{\text{meas}} = \sum_{hkl} [N(hkl)/[N(hkl) - 1]]^{1/2} \sum_i |I_i(hkl) - \langle I(hkl) \rangle| / \sum_{hkl} \sum_i I_i(hkl)$ , where  $I_i(hkl)$  is the observed intensity and  $\langle I(hkl) \rangle$  is the average intensity from  $N(hkl)$  observations (symmetry-related and duplicate measurements of a unique reflection). <sup>‡</sup>  $R_{\text{p.i.m.}} = \sum_{hkl} [1/[N(hkl) - 1]]^{1/2} \sum_i |I_i(hkl) - \langle I(hkl) \rangle| / \sum_{hkl} \sum_i I_i(hkl)$ . <sup>§</sup> CC<sub>1/2</sub> values are the half-set correlation coefficients (Karplus & Diederichs, 2012). <sup>¶</sup>  $R_{\text{cryst}} = \sum_{hkl} |F_{\text{obs}}| - |F_{\text{calc}}| / \sum_{hkl} |F_{\text{obs}}|$ ;  $R_{\text{free}}$  is calculated for a randomly selected 5% of reflections that were excluded from refinement. <sup>††</sup> Root-mean-square deviation from ideal values.

concentrated by centrifugation; their concentration was determined by measuring the absorbance at 280 nm with a NanoDrop 2000 (Thermo Scientific).

### 2.5. Biolayer interferometry (BLI)

The proteins were biotinylated using the EZ-Link NHS-PEG4-Biotin kit (Perbio Science, France). The reaction was quenched by removing the excess biotin using a Zeba Spin Desalting column (Perbio Science, France) which was equilibrated with PBS buffer. BLI studies were performed in black 96-well plates (Greiner) at 25°C using an Octet RED96 (ForteBio, USA; PBS, 0.01% BSA, 0.002% Tween 20, 0.005% sodium azide). Streptavidin biosensor tips (ForteBio, USA) were first hydrated with 0.2 ml kinetic buffer (KB; ForteBio, USA; PBS, 0.01% BSA, 0.002% Tween20 and 0.005% sodium azide) for 20 min and then loaded with biotinylated pPorM-Nter, pPorM-Cter or pPorM (10 µg ml<sup>-1</sup> in KB). The surface was then blocked using biocytin. The association of PorM with various concentrations of nanobodies (a zero concentration and concentrations varying from 0.5 to 250 nM, depending on the experiment) was monitored for 300 s, and the dissociation was followed for 600 or 900 s. in KB. These experiments were run two times independently. Control experiments were run to check that there was no nonspecific interaction between the analytes (nanobodies) and control biosensors (loaded with no protein and blocked with biocytin). Fitting of the binding data and the measurement of constants were performed with the Octet RED system software (v.7.1) using a 1:1 model. The error values are calculated from two independent experiments; averaged statistical parameters ( $\chi^2$  and  $R^2$ ) generated during the fittings are reported.

### 2.6. Crystallization, data collection and processing

Initial crystallization trials of the nanobodies and of their complexes with PorM constructs were performed by the sitting-drop vapour-diffusion method at 293 K in 96-well Greiner plates using a Mosquito Crystal robot (TTP Labtech

with the following screens: Wizard I and II (Rigaku Reagents), JCSG+ (Qiagen), Index (Hampton Research), Crystal Screen and Crystal Screen 2 (Hampton Research). Drops were prepared by mixing different volumes (100, 200 and 300 nl) of protein solution and 100 nl precipitant solution and were equilibrated against a 150 µl reservoir volume. Initial crystallization conditions were obtained in several conditions. For nb19 only, optimization was then carried out by varying the pH and the concentration of the precipitant (Lartigue *et al.*, 2003). The final crystallization conditions are given in Table 1. Crystals were mounted in cryoloops (Hampton CrystalCap Magnetic) and were briefly soaked in crystallization solution supplemented with the appropriate cryoprotectant before being flash-cooled in a nitrogen-gas stream at 100 K using a home cryocooling device (Oxford Cryosystems). For the nb130-pPorM-Cter complex, a 5 min air-dehydration step was performed in the crystallization solution with a 10% increase in the precipitant concentration and supplemented with the cryoprotectant.

Diffraction data were collected on beamlines ID23 and ID29 at the European Synchrotron Research Facility (ESRF), Grenoble, France and on PROXIMA-1 and PROXIMA-2 at SOLEIL, Paris, France. The data sets were integrated with XDS (Kabsch, 2010) and were scaled with SCALA (Evans, 2006) from the CCP4 suite (Winn *et al.*, 2011). Data-collection statistics are reported in Table 1. The Matthews coefficient and solvent content were calculated with MATTHEWS\_COEF (Kantardjiev & Rupp, 2003) from the CCP4 suite.

### 2.7. Molecular replacement and refinement

Molecular replacement was performed with MOLREP (Vagin & Teplyakov, 2010) from the CCP4 suite. A different starting model was used for each nanobody, according to the result of sequence alignment against the wwPDB. For nb01, nb02 and nb130 molecular replacement was straightforward. For nb19, MOLREP returned a well contrasted solution for three VHHs. After refinement with autoBUSTER (Blanc *et*

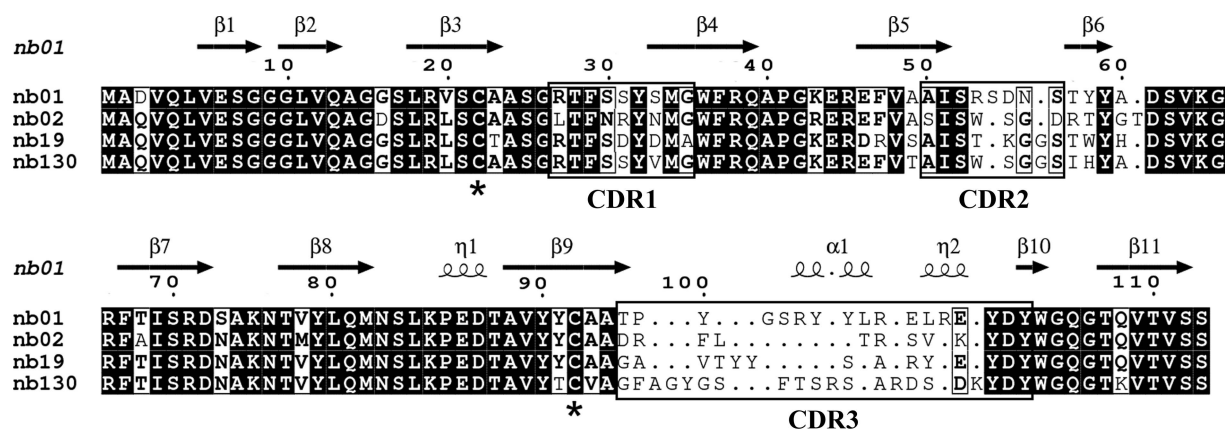


**Figure 1**  
Sequence alignment of the four nanobodies nb01, nb02, nb19 and nb130 raised against the periplasmic domain of PorM. Secondary-structure elements from the nb01 structure (molecule A) are displayed above the alignment. The CDR1, CDR2 and CDR3 sequences are boxed; the cysteine residues are denoted by asterisks. Kabat numbering is used (Kabat *et al.*, 1991). The sequence alignment was generated by DeepAlign (Wang *et al.*, 2013) on the basis of the superposition of the four nanobody structures (molecule A for nb01 and nb19) and processed by ESPript (Robert & Gouet, 2014).

**Table 2**

Kinetic and thermodynamic parameters of the interactions between the nanobodies nb01, nb02, nb19 and nb130 with different constructs of the PorM periplasmic domain.

	$K_d$ (nM)	$K_{ass}$ ( $M^{-1} s^{-1}$ )	$K_{diss}$ ( $s^{-1}$ )	Full $\chi^2$ – full $R^2$
pPorM–nb01	1.8 ± 0.7	8.1 ± 2.4 × 10 <sup>5</sup>	1.4 ± 0.2 × 10 <sup>−3</sup>	1.38–0.98
pPorM–nb02	2.5 ± 1.5	3.1 ± 1.0 × 10 <sup>5</sup>	7.7 ± 1.5 × 10 <sup>−4</sup>	1.88–0.98
pPorM–nb19	3.8 ± 1.4	1.7 ± 0.4 × 10 <sup>5</sup>	6.7 ± 0.6 × 10 <sup>−4</sup>	0.35–0.98
pPorM–nb130	4.5 ± 1.0	1.4 ± 0.3 × 10 <sup>5</sup>	6.3 ± 0.3 × 10 <sup>−4</sup>	1.29–0.99
pPorM–Nter–nb01	4.0 ± 1.1	2.0 ± 0.7 × 10 <sup>5</sup>	8.0 ± 0.8 × 10 <sup>−4</sup>	3.49–0.99
pPorM–Nter–nb02	5.5 ± 1.2	1.6 ± 0.5 × 10 <sup>5</sup>	9.0 ± 0.6 × 10 <sup>−4</sup>	3.98–0.99
pPorM–Cter–nb19	8.6 ± 1.4	6.7 ± 1.5 × 10 <sup>4</sup>	5.8 ± 0.2 × 10 <sup>−4</sup>	5.44–0.99
pPorM–Cter–nb130	8.0 ± 1.5	6.8 ± 1.2 × 10 <sup>4</sup>	5.6 ± 0.2 × 10 <sup>−4</sup>	4.97–0.99

*al.*, 2004), electron density for a fourth VHH could be identified. However, even using the refined model of the three VHs, *MOLREP* could not localize this fourth VHH. The amino-acid chain was therefore traced manually with *TURBO* (Roussel & Cambillau, 1991) until there was sufficient structural information to allow the positioning of a complete VHH by rotation/translation.

Refinement of the four-nanobody model was performed with *autoBUSTER* and *PHENIX* (Adams *et al.*, 2010), and the structures were corrected with *Coot* (Emsley *et al.*, 2010). Model validations were performed with *MolProbity* (Chen *et al.*, 2010). Refinement statistics are reported in Table 1.

### 3. Results

#### 3.1. Nanobody generation and binding characterization

Nanobodies were raised by immunization of llamas with the purified periplasmic domain of the PorM protein (residues

36–516; pPorM). Several strong pPorM binders were identified from the immune library by three rounds of panning using phage display coupled to ELISA. Four nanobodies, called nb01, nb02, nb09 and nb130, were selected for further study based on their high affinity for pPorM and on their amino-acid differences in the variable regions [also called the complementarity-determining regions (CDRs); Fig. 1]. Interestingly, nb02, nb19 and nb130 were also present in a naïve library generated in the laboratory (article in preparation). The four nanobodies possess the two cysteines Cys22 and Cys92 that form the conserved disulfide bond that is present in all VHH domains. The CDR1 and CDR2 of the four nanobodies have the same length (nine and eight residues, respectively), but there is a great variation in the length of the CDR3: 17, 12, 14 and 21 residues for nb01, nb02, nb19 and nb130, respectively.

The nanobodies were produced in the periplasm of *Escherichia coli* and purified to homogeneity. They all behaved as monomers in size-exclusion chromatography. In a previous study (Stathopoulos *et al.*, 2015), we have shown that a fragment of the purified pPorM could be obtained by limited proteolysis (hereafter denoted pPorM-T). Using N-terminal Edmann sequencing and peptide mass fingerprinting (results not shown), we deduced that this fragment corresponds to the C-terminal part of pPorM (residues 225–516; hereafter denoted pPorM-Cter). We then produced this domain as well as the remaining N-terminal part of pPorM (residues 44–217; hereafter denoted pPorM-Nter), and their interaction with the four nanobodies was assessed by biolayer interferometry (BLI). The four nanobodies bind to pPorM in the nanomolar range. Interestingly, they present a specificity in their interaction with pPorM: nb01 and nb02 bind specifically to

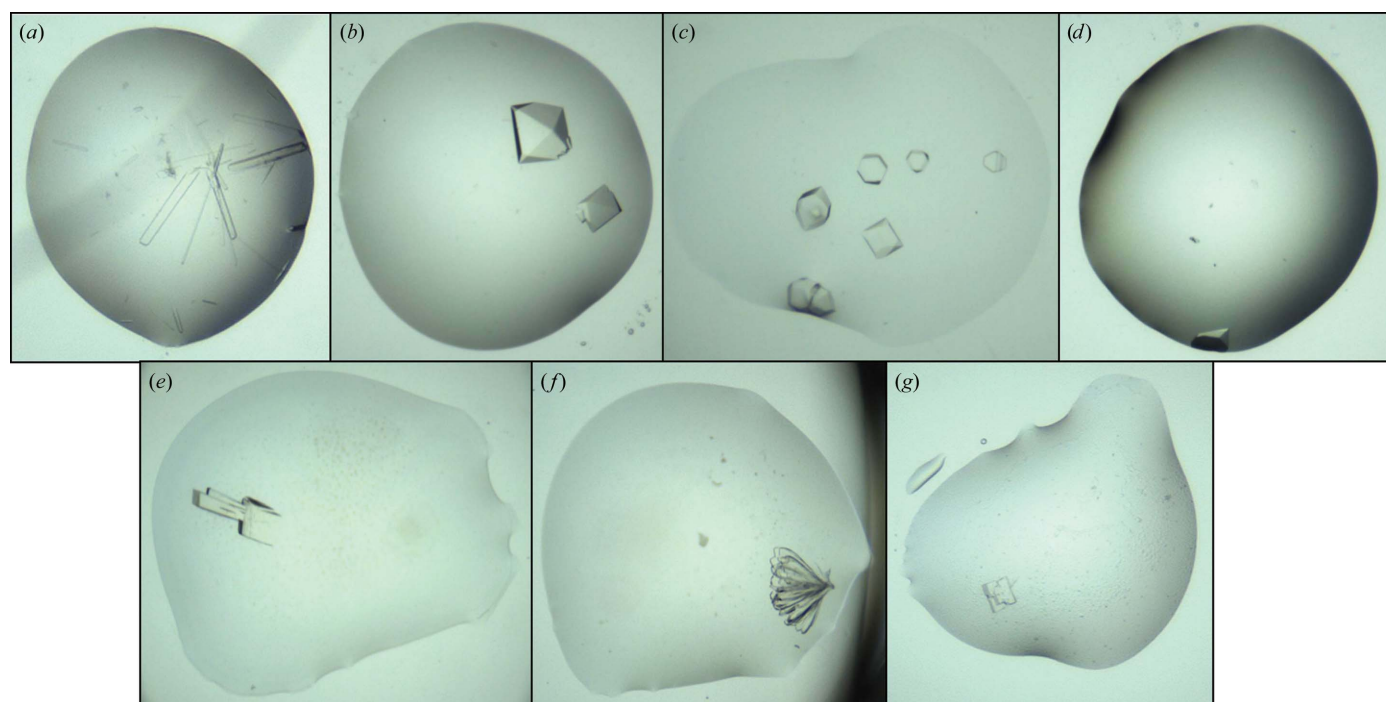


**Figure 2**

Crystals of nb01 (a), nb02 (b), nb19 (c) and nb130 (d), of pPorM-Cter in complex with nb130 in space group  $P2_1$  (e) and space group  $P2$  (f), and of pPorM-Nter in complex with nb01 (g).

pPorM-Nter, whereas nb19 and nb130 bind specifically to pPorM-Cter. The results are summarized in Table 2.

### 3.2. Nanobody structures

We decided to solve the structures of the four nanobodies alone for the following two reasons. On one hand, high-resolution structures of the nanobodies could be used either to solve the structure of the complex with the protein of interest by molecular replacement or to help in building in the case of *ab initio* phasing. On the other hand, as there are only a limited number of unbound nanobody structures in the PDB, new structures will provide more data for potential use in theoretical studies of single-chain antibody binding. Thus, the four nanobodies were crystallized (Fig. 2) and their structures were solved by molecular replacement. As expected, the four nanobodies adopt the classical immunoglobulin fold (Fig. 3) with two  $\beta$ -sheets composed of four antiparallel  $\beta$ -strands:

$\beta 1-\beta 3-\beta 7-\beta 8$  and  $\beta 4-\beta 5-\beta 6-\beta 9$ . The former  $\beta$ -sheet is flanked by CDR3 and is further prolonged by two parallel  $\beta$ -strands ( $\beta 2$  and  $\beta 11$ ). One  $\pi$ -helix is present in the  $\beta 8-\beta 9$  loop. The structures of the four nanobodies display a high level of homology, with an r.m.s.d. ranging from 0.69 to 0.99 Å on C $\alpha$  atoms without the CDRs. The main differences arise from the CDRs, which are located at the N-terminal edge of the  $\beta$ -sandwich. Indeed, CDR3, which generally mediates interaction with the epitope, is the most divergent. Its folding is different in the four structures: one  $\alpha$ -helix and one  $\pi$ -helix in nb01, random coil only in nb02, random coil only or prolonged  $\beta$ -strands in nb19 and one  $\pi$ -helix in nb130 (Fig. 3). Paradoxically, the long CDR3s of nb01 and nb130 (17 and 21 residues, respectively) adopt a unique conformation in the crystal, suggesting a certain conformational stability. On the contrary, despite its shorter sequence (14 residues), the CDR3 of nb19 is more flexible, as it can adopt multiple distinct conformations. The CDR3 conformational heterogeneity

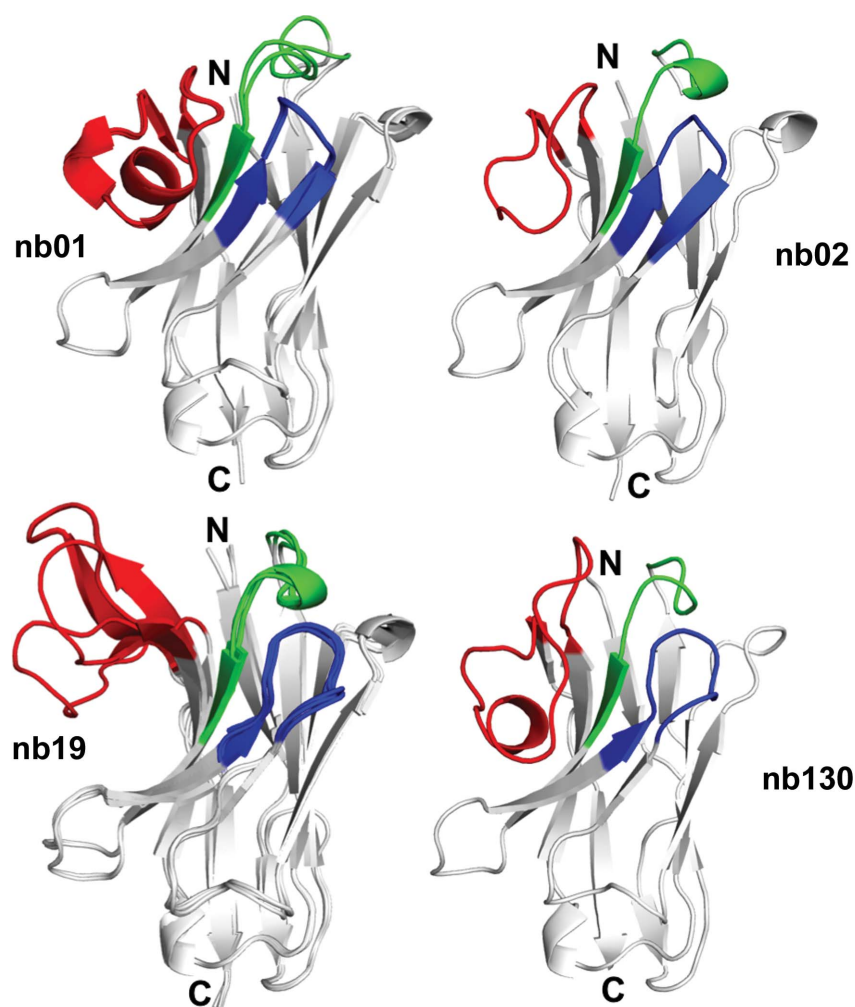


Figure 3

Crystal structures of the four nanobodies nb01, nb02, nb19 and nb130 raised against the periplasmic domain of PorM. CDR1, CDR2 and CDR3 of each nanobody according to Kabat numbering (Kabat *et al.*, 1991) are represented in green, blue and red, respectively. The N- and C-terminal extremities are labelled N and C, respectively. The different molecules present in the asymmetric unit are superposed (molecules A and B of nb01 and molecules A, B and D of nb19; molecule C of nb19, which is identical to molecule B, is not represented for the purposes of clarity). This figure was generated by PyMOL (Schrödinger).

observed only in nb19 could be related to the substitution of the Phe47 present in nb01, nb02 and nb130 by an arginine residue in nb19 (Fig. 1). Indeed, the CDR3 of nb01, nb02 and nb130 folds over and packs against the hydrophobic side chain of the framework Phe47, while the CDR3 of nb19 is somewhat repulsed by the side chain of Arg47.

### 3.3. Use of nanobodies as crystallization chaperones

We have previously obtained diffracting crystals of pPorM-T and of its selenomethionine derivative; native and MAD data sets were collected and an experimental map was calculated (Stathopoulos *et al.*, 2015). However, building of the C-terminal domain of pPorM-T was challenging, probably owing to the higher thermal motion of this domain. We decided to use nanobodies as crystallization chaperones, with the assumption that complex formation may minimize the conformational flexibility of the target. Therefore, crystallization trials of pPorM-Cter in complex with its specific nanobodies nb19 and nb130 were performed. Crystals of pPorM-Cter in complex with nb130 were obtained in space groups  $P2$  and  $P2_1$  that diffracted to 2.5 and 2.15 Å resolution, respectively (Fig. 2). In an attempt to improve the resolution, the  $P2_1$  crystals were dehydrated, resulting in crystals in a new space group,  $P1$ , that diffracted to 2.1 Å resolution. Structure determination of the complex is in progress using the nb130 structure and the partial model of pPorM-T as a model for molecular replacement.

The same strategy of co-crystallization with nanobodies was applied in order to overcome our inability to obtain exploitable pPorM-Nter crystals. Indeed, all of the native or selenomethionine-derivative crystals that we obtained for this construct were twinned and therefore were not usable to solve the structure *ab initio*. Crystallization trials of complexes with nb01 or nb02 were then performed and crystals of pPorM-Nter in complex with nb01 were obtained that diffracted to 2.4 Å resolution (Fig. 2).

## 4. Concluding remarks

In recent years, nanobodies have been intensively used as crystallization chaperones in structural studies. Indeed, they preferentially bind concave and hinge regions of proteins and thus can help in the crystallization process of recalcitrant targets such as multi-domain proteins, large complexes and membrane proteins (Desmyter *et al.*, 2015). In our case, nanobodies also turned out to be valuable tools in the structure-determination process. For pPorM-Cter, co-crystallization with the nanobody nb130 permitted the resolution of the structure to be increased, presumably by stabilizing a flexible domain of the protein. For pPorM-Nter, co-crystallization with the nanobody nb01 permitted us to obtain untwinned crystals, in contrast to the protein alone. Molecular replacement was performed with the structure of the nanobody as a starting model, providing the initial phases used to calculate electron-density maps. Recently, we solved the structure of a truncated construct of TssM using the same

strategy. TssM is a central component of the membrane complex of the type VI secretion system. The construct TssM<sub>32Ct</sub> (residues 836–1129 of the TssM periplasmic domain) was co-crystallized with a specific nanobody (Nguyen *et al.*, 2015) and its structure was built into the electron-density maps obtained after molecular replacement using the structure of the nanobody as a starting model (Durand *et al.*, 2015). As pPorM-Nter is smaller than TssM<sub>32Ct</sub> (211 and 293 residues, respectively) and as the crystals of the two proteins in complex with their respective nanobodies diffracted to similar resolutions (2.4 Å for pPorM-Nter and 1.92 Å for TssM<sub>32Ct</sub>), we are confident that we will succeed in building the structure of pPorM-Nter.

## Acknowledgements

We would like to thank the European Synchrotron Research Facility (ESRF) and the SOLEIL synchrotron for beamline allocation.

## Funding information

Funding for this research was provided by: Centre National de la Recherche Scientifique; French Infrastructure for Integrated Structural Biology (FRISBI) (award No. ANR-10-INSB-05-01); Agence Nationale de la Recherche (award No. ANR-15-CE11-0019-01); Ministère de l'Éducation Nationale, de l'Enseignement Supérieur et de la Recherche (award No. doctoral fellowship for YD); Région PACA (award No. doctoral fellowship for JR); Eiffel program from the French Ministère des Affaires Étrangères (award No. doctoral fellowship for TNTT).

## References

- Adams, P. D. *et al.* (2010). *Acta Cryst.* **D66**, 213–221.
- Arbabi Ghahroudi, M., Desmyter, A., Wyns, L., Hamers, R. & Muyldermans, S. (1997). *FEBS Lett.* **414**, 521–526.
- Armitage, G. C. (1996). *Ann. Periodontol.* **1**, 37–215.
- Blanc, E., Roversi, P., Vonrhein, C., Flensburg, C., Lea, S. M. & Bricogne, G. (2004). *Acta Cryst.* **D60**, 2210–2221.
- Conrath, K., Pereira, A. S., Martins, C. E., Timóteo, C. G., Tavares, P., Spinelli, S., Kinne, J., Flaudrops, C., Cambillau, C., Muyldermans, S., Moura, I., Moura, J. J. G., Tegoni, M. & Desmyter, A. (2009). *Protein Sci.* **18**, 619–628.
- Chen, V. B., Arendall, W. B., Headd, J. J., Keedy, D. A., Immormino, R. M., Kapral, G. J., Murray, L. W., Richardson, J. S. & Richardson, D. C. (2010). *Acta Cryst.* **D66**, 12–21.
- Desmyter, A., Farenc, C., Mahony, J., Spinelli, S., Bebeacqua, C., Blangy, S., Veesler, D., van Sinderen, D. & Cambillau, C. (2013). *Proc. Natl Acad. Sci. USA*, **110**, E1371–E1379.
- Desmyter, A., Spinelli, S., Roussel, A. & Cambillau, C. (2015). *Curr. Opin. Struct. Biol.* **32**, 1–8.
- Desmyter, A., Transue, T. R., Ghahroudi, M. A., Dao Thi, M.-H., Poortmans, F., Hamers, R., Muyldermans, S. & Wyns, L. (1996). *Nature Struct. Mol. Biol.* **3**, 803–811.
- Durand, E., Nguyen, V. S., Zoued, A., Logger, L., Péhau-Arnaudet, G., Aschtgen, M.-S., Spinelli, S., Desmyter, A., Bardiaux, B., Dujancourt, A., Roussel, A., Cambillau, C., Cascales, E. & Fronzes, R. (2015). *Nature (London)*, **523**, 555–560.
- Emsley, P., Lohkamp, B., Scott, W. G. & Cowtan, K. (2010). *Acta Cryst.* **D66**, 486–501.
- Evans, P. (2006). *Acta Cryst.* **D62**, 72–82.

- Hamers-Casterman, C., Atarhouch, T., Muyldermans, S., Robinson, G., Hammers, C., Songa, E. B., Bendahman, N. & Hammers, R. (1993). *Nature (London)*, **363**, 446–448.
- Kabat, E. A., Wu, T. T., Perry, H. M., Gottesmann, K. S. & Foeller, C. (1991). *Sequences of Proteins of Immunological Interest*, 5th ed. Bethesda: National Institutes of Health.
- Kabsch, W. (2010). *Acta Cryst.* **D66**, 133–144.
- Kantardjieff, K. A. & Rupp, B. (2003). *Protein Sci.* **12**, 1865–1871.
- Karplus, P. A. & Diederichs, K. (2012). *Science*, **336**, 1030–1033.
- Lartigue, A., Gruez, A., Briand, L., Pernollet, J.-C., Spinelli, S., Tegoni, M. & Cambillau, C. (2003). *Acta Cryst.* **D59**, 919–921.
- Nguyen, V. S., Spinelli, S., Desmyter, A., Le, T. T. H., Kellenberger, C., Cascales, E., Cambillau, C. & Roussel, A. (2015). *Acta Cryst.* **F71**, 266–271.
- Robert, X. & Gouet, P. (2014). *Nucleic Acids Res.* **42**, W320–W324.
- Roussel, A. & Cambillau, C. (1991). *Silicon Graphics Geometry Partners Directory*, p. 81. Mountain View: Silicon Graphics.
- Sato, K., Naito, M., Yukitake, H., Hirakawa, H., Shoji, M., McBride, M. J., Rhodes, R. G. & Nakayama, K. (2010). *Proc. Natl Acad. Sci. USA*, **107**, 276–281.
- Spinelli, S., Frenken, L., Bourgeois, D., de Ron, L., Bos, W., Verrips, T., Anguille, C., Cambillau, C. & Tegoni, M. (1996). *Nature Struct. Biol.* **3**, 752–757.
- Stathopoulos, J., Cambillau, C., Cascales, E., Roussel, A. & Leone, P. (2015). *Acta Cryst.* **F71**, 71–74.
- Vagin, A. & Teplyakov, A. (2010). *Acta Cryst.* **D66**, 22–25.
- Vincent, M. S., Canestrari, M. J., Leone, P., Stathopoulos, J., Ize, B., Zoued, A., Cambillau, C., Kellenberger, C., Roussel, A. & Cascales, E. (2017). *J. Biol. Chem.* **292**, 3252–3261.
- Wang, S., Ma, J., Peng, J. & Xu, J. (2013). *Sci. Rep.* **3**, 1448.
- Winn, M. D. *et al.* (2011). *Acta Cryst.* **D67**, 235–242.